



The study of angular momentum on the fusion of $^{28}_{14}\text{Si}+^{28}_{14}\text{Si}$, using SEDF in semiclassical extended Thomas-Fermi approach

Vivek Kumar Nautiyal^{a,*}, Atul Choudhary^b, Bipin Singh Koranga^c,
Agam Kumar Jha^c

^a Department of Physics, Chaudhary Charan Singh University, Meerut, (U.P.)-250004, India

^b Department of Physics, Government Degree College, Banjar, Kullu, (H.P.)-175123, India

^c Department of Physics, Kirori Mal college (University of Delhi), Delhi-110007, India

Received 21 February 2023; received in revised form 11 April 2023; accepted 2 May 2023

Available online 5 May 2023

Abstract

The total fusion cross-sections are calculated for energies both above and below the potential barrier by using the properties of the interaction potential in Hill-Wheeler approximation for a positive Q-value system $^{28}_{14}\text{Si}+^{28}_{14}\text{Si}$. The Coulomb and centrifugal parts of the potentials are added directly to the nuclear proximity potential to calculate the total interaction potential, where nuclear proximity potential is obtained in semiclassical extended Thomas-Fermi approach of Skyrme energy density formalism for Skyrme SIV parametrization. The angular momentum spectrum of total cross sections is obtained and calculated by using angular momentum dependent properties of the total interaction potential. The properties of total interaction potential, which are usually treated as independent of angular momentum, i.e. barrier height, barrier position and its width are calculated and found to depend sharply on the angular momentum value at a fixed center of mass energy. It effect the fusion cross-section sufficiently above the barrier energy. However at energies below the barrier energy the addition of large angular momentum values have negligible effects on fusion cross-section. Further, the maximum in fusion cross-section is observed at a particular value of angular momentum, which is not equal to the maximum value of angular momentum.

© 2023 Elsevier B.V. All rights reserved.

* Corresponding author.

E-mail addresses: viveknautiyal01@gmail.com (V.K. Nautiyal), choudharyatul786@gmail.com (A. Choudhary), bpiniitb@rediffmail.com (B.S. Koranga), agamjha_2001@yahoo.co.in (A.K. Jha).

Keywords: Thomas Fermi; SEDF; Skyrme

1. Introduction

Recently in an experiment [1] the total fusion cross-section is measured for $^{28}_{14}\text{Si}+^{28}_{14}\text{Si}$ ($Q_{in} = 10.9$ MeV), at Laboratori Nazionali di Legnaro of Italian Institute of Nuclear Physics (INFN), at energies close and below the barrier upto 600 nb. The data of the experiment in comparison with calculations has shown that the calculated fusion cross-section is overestimated in coupled channel (CC) framework, except for low energies. In order to describe the observed behavior in the fusion cross-section the parameters of the interaction potential i.e. M3Y+repulsion, were adjusted to fit the data. Similarly to predict the form of nuclear potential, in an earlier work [2], has reanalyzed the data for the same system within same framework of CC by using the experimental data of Refs. [3–5] and more data with higher precision is expected to explain the observed behavior at above barrier energies. It indicates that for the study of the total fusion cross-section the search for an appropriate potential is still a matter of great interest. So it will be interesting to see the effect of interaction potential obtained from semiclassical extended Thomas-Fermi approach of Skyrme energy density formalism (SEDF) on fusion cross section of the system $^{28}_{14}\text{Si}+^{28}_{14}\text{Si}$ ($Q_{in} = 10.9$ MeV). Since SEDF has ability to give different kind of nuclear potential for different Skyrme forces, but here we have used Skyrme force SIV, because it has found be in agreement with fusion data, except at energies [7] above the barrier. So we can study fusion cross-section at these energies by using the above mentioned total interaction potential and its properties.

In the present work, the Coulomb and centrifugal potentials are added directly to the nuclear proximity potential to obtain and calculate total nuclear potential and hence its properties are utilized to obtain fusion cross-section. The nuclear(proximity) potential is calculated by using semiclassical extended Thomas-Fermi (ETF) of SEDF for Skyrme force SIV. This approach at ETF level contains the second and higher order contribution of order parameter \hbar , for both kinetic as well spin orbit energy density [8,9] but here the calculations are restricted upto second order which is found to have good numerical convergence [10]. Further for the calculations of the nuclear density we have used the temperature dependent two parameter Thomas-Fermi density [11,12] with in slab approximation. The parameters of TF density are taken from Ref [13] while their temperature dependence is taken from Ref [14]. Since addition of the angular momentum based potential (i.e. centrifugal potential), equivalent repulsive nuclear potential, so it gives different kind of interaction potential for different partial waves or different l -values). So it gives an opportunity to study the effect of angular momentum based total potential on the study of fusion cross sections.

In calculations of the fusion cross-section depending upon the angular momentum we have used the Hill-Wheeler (HW) formula [15] for each partial wave. Since in HW approximation the tunneling probability can be calculated for the penetration of each of the partial wave at a given energy so it provides a simple formula for fusion cross-section depending upon angular momentum at a given energy. The fusion cross section obtained through HW approximation are calculated here in two ways, in the first way all the barrier properties namely barrier height, barrier curvature/width and barrier position, are taken as function of angular momentum while in other case only barrier height is taken as variable. The reason for considering the second case is based on the approximation which is used in refs. [2,16] to calculate the height of the interaction barriers. Then so obtained fusion cross-sections are compared with data of Ref. [1]

and recently available data of Ref. [6] over all the available energy range. In the earlier case, we calculated fusion cross section for each of the partial wave upto a certain value of angular momentum and then summed up cross section is calculated by summing individual cross-sections. The comparison of calculated fusion cross-section with the experimentally measured data [1,6] allowed us to approximately assign maximum value to angular momentum which is required to reproduce the data with in experimental limit of error over all the energy range available.

The paper is organized in various sections as, Sec 2 describe the model way of calculation of total interaction potential as function of inter-nuclear distance and fusion cross-section using angular momentum (ℓ) dependent HW approximation. Sec 3, starts with discussion that how the addition of angular momentum based potential effects the properties of total interaction potential and then these effects are inculcated in fusion cross-sections calculations as a function of angular momentum and is shown graphically. Finally section 4, concludes with significance of incorporating the angular momentum effect along with HW approximation.

2. Methodology

In this section we have discussed the details of the method which is used in the calculation of the fusion cross section depending upon angular momentum (ℓ) and center of mass energy (E_{cm}). The total fusion cross-section is obtained and calculated by using the properties of the total interaction potential. The Coulomb and centrifugal parts of the potentials are added directly to the nuclear proximity potential to calculate the total interaction potential, where nuclear proximity potential is obtained in semiclassical extended Thomas-Fermi approach of Skyrme energy density formalism for Skyrme SIV parametrization.

In SEDF, the nuclear interaction potential as a function of inter-nuclear separation which is defines as the difference between the energy average value of the two nuclei that are overlapping (at a finite separation distance R) and are completely separated (at $R = \infty$) and is,

$$V(R) = E(R) - E(\infty) \quad (1)$$

where $E = \int H(\vec{r})d^3\vec{r}$, is the energy average value of Skyrme Hamiltonian density (for details see refs. [13,17]), and is

$$\begin{aligned} H = & \frac{\hbar^2}{2m}\tau_q + \frac{1}{2}t_0 \left[\left(1 + \frac{x_0}{2}\right)\rho^2 - \left(x_0 + \frac{1}{2}\right)(\rho_n^2 + \rho_p^2) \right] \\ & + \frac{1}{12}t_3\rho^{\alpha_0} \left[\left(1 + \frac{x_3}{2}\right)\rho^2 - \left(x_3 + \frac{1}{2}\right)(\rho_n^2 + \rho_p^2) \right] \\ & + \frac{1}{4} \left[t_1 \left(1 + \frac{x_1}{2}\right) + t_2 \left(1 + \frac{x_2}{2}\right) \right] \rho\tau \\ & - \frac{1}{4} \left[t_1 \left(x_1 + \frac{1}{2}\right) - t_2 \left(x_2 + \frac{1}{2}\right) \right] (\rho_n\tau_n + \rho_p\tau_p) \\ & + \frac{1}{16} \left[3t_1 \left(1 + \frac{x_1}{2}\right) - t_2 \left(1 + \frac{x_2}{2}\right) \right] (\vec{\nabla}\rho)^2 \\ & - \frac{1}{16} \left[3t_1 \left(x_1 + \frac{1}{2}\right) + t_2 \left(x_2 + \frac{1}{2}\right) \right] \left\{ (\vec{\nabla}\rho_p)^2 + (\vec{\nabla}\rho_n)^2 \right\} \\ & - \frac{1}{2}W_0 \left[\rho\vec{\nabla}\cdot\vec{J} + \rho_n\vec{\nabla}\cdot\vec{J}_n + \rho_p\vec{\nabla}\cdot\vec{J}_p \right] \end{aligned} \quad (2)$$

where $\vec{J} = \vec{J}_n + \vec{J}_p$, $\rho = \rho_p + \rho_n$, $\tau = \tau_p + \tau_n$, are the spin-orbit, nuclear, and kinetic energy densities respectively, x_i , t_i , α_0 , and W_0 are the Skyrme force parameters, fitted by different authors, (for detail see refs. [9,18]) for the ground state properties of the nuclei.

The kinetic energy density term, τ_q , is in second order of expansion (enough for numerical convergence [10]), is

$$\begin{aligned} \tau_q(\vec{r}) &= \frac{3}{5} \left(3\pi^2\right)^{2/3} \rho_q^{5/3} + \frac{1}{36} \frac{(\vec{\nabla}\rho_q)^2}{\rho_q} + \frac{1}{3} \Delta\rho_q \\ &+ \frac{1}{6} \frac{\vec{\nabla}\rho_q \cdot \vec{\nabla}f_q + \rho_q \Delta f_q}{f_q} - \frac{1}{12} \rho_q \left(\frac{\vec{\nabla}f_q}{f_q}\right)^2 \\ &+ \frac{1}{2} \rho_q \left(\frac{2m}{\hbar^2}\right)^2 \left(W_0 \frac{\vec{\nabla}(\rho + \rho_q)}{2f_q}\right)^2 \end{aligned} \quad (3)$$

the effective mass form factor is $f_q(\vec{r})$, which is function of effective mass term ($m^*(\vec{r})$) is:

$$\begin{aligned} f_q(\vec{r}) &= \frac{m}{m^*(\vec{r})} \\ &= 1 + \frac{2m}{\hbar^2} \frac{1}{4} \left\{ t_1 \left(1 + \frac{x_1}{2}\right) + t_2 \left(1 + \frac{x_2}{2}\right) \right\} \\ &- \frac{2m}{\hbar^2} \frac{1}{4} \left\{ t_1 \left(x_1 + \frac{1}{2}\right) - t_2 \left(x_2 + \frac{1}{2}\right) \right\} \rho_q(\vec{r}) \end{aligned} \quad (4)$$

where $q = p$ or n for proton (or neutron). The spin \vec{J} has no contribution at the semiclassical functional in the lowest order, the second order contribution is,

$$\vec{J}_q(\vec{r}) = -\frac{2m}{\hbar^2} \left(\frac{1}{2}W_0\right) \frac{1}{f_q} \rho_q \vec{\nabla}(\rho + \rho_q) \quad (5)$$

The nuclear interaction potential between the two interacting nuclei is given as,

$$V_N(R) = \int [H(\vec{J}, \rho, \tau) - \{H_1(\vec{J}_1, \rho_1, \tau_1) + H_2(\vec{J}_2, \rho_2, \tau_2)\}] d^3r$$

where $\vec{J} = \vec{J}_1 + \vec{J}_2$, $\rho = \rho_1 + \rho_2$, and $\tau = \tau_1 + \tau_2$ for the composite system, in the sudden approximation. The nuclear potential (with in slab approximation) becomes (for detail see refs. [12,13]),

$$V_N(R) = 2\pi \bar{R} \int_{s_0}^{\infty} e(s) ds, \quad (6)$$

where $\bar{R} = R_{01}R_{02}/(R_{01} + R_{02})$ is the mean curvature radius/geometrical factor, R_{0i} are the central radii of interacting nuclei and $e(s)$ is the interaction energy per unit area between two flat slabs of semi-infinite nuclear matter with surfaces parallel to the $x - y$ plane and moving in the z -direction separated by distance s , having a minimum value s_0 , is given by,

$$\begin{aligned} \int_{s_0}^{\infty} e(s) ds &= \int [H(\vec{J}, \rho, \tau) - \{H_1(\vec{J}_1, \rho_1, \tau_1) \\ &+ H_2(\vec{J}_2, \rho_2, \tau_2)\}] dz. \end{aligned} \quad (7)$$

As \vec{J} and τ , both depends upon ρ , so H becomes function of ρ only. Since both spin-orbit density independent part (attractive) and dependent (repulsive) acts differently, so Eq. (6) can be expressed as,

$$V_N(R) = V_P(R) + V_J(R) \quad (8)$$

Then the total nuclear potential ($V_T(R)$) is obtained by adding explicitly the Coulomb potential ($V_C(R) = 1.44Z_1Z_2/R$), the centrifugal potential part ($V_\ell(R) = \hbar^2\ell(\ell + 1)/2\mu R^2$) to the nuclear proximity potential ($V_N(R)$).

The nuclear matter density, $\rho_i = \rho_{n_i} + \rho_{p_i}$, where $\rho_{n_i} = (N_i/A_i)\rho_i$ and $\rho_{p_i} = (Z_i/A_i)\rho_i$, $i = 1, 2$ for the two overlapping nuclei [13], is the two parameter Thomas-Fermi density as a function of temperature with in the slab approximation is,

$$\rho_i(z_i, T) = \rho_{0i}(T) \left[1 + \exp\left(\frac{z_i - R_{0i}(T)}{a_{0i}(T)}\right) \right]^{-1} \quad (9)$$

with $-\infty \leq z \leq \infty$ and $z_2 = R - z_1$, and central density is,

$$\rho_{0i}(T) = \frac{3A_i}{4\pi R_{0i}^3(T)} \left[1 + \frac{\pi^2 a_{0i}^2(T)}{R_{0i}^2(T)} \right]^{-1} \quad (10)$$

The temperature dependence or the effect of center of mass energy is included through the two parameters of the two parameter Thomas-Fermi density. The temperature T (in MeV) is related to the center of mass energy (E_{cm}) as,

$$E_{CN}^* = E_{cm} + Q_{in} = \left(\frac{A}{9}\right) T^2 - T \quad (11)$$

where E_{CN}^* is compound nucleus excitation energy and Q_{in} is the Q-value of reaction, A is the mass number of the fused system. The central radii $R_{0i}(T = 0)$, surface thicknesses $a_{0i}(T = 0)$ are taken from ref. [13], while their temperature dependence is taken from ref. [14].

The fusion cross-section as a function of center of mass energy (E_{cm}) in the partial wave analysis is defined as,

$$\sigma_f(E_{cm}, \ell) = \frac{\pi \hbar^2}{2\mu E_{cm}} \sum_{\ell=0}^{\ell_{max}} (2\ell + 1) P(E_{cm}, \ell) \quad (12)$$

where $P(E_{cm}, \ell)$ is the penetration probability in Hill-Wheeler approximation [15] for a given partial wave and center of mass energy and is,

$$P_{HW}(E_{cm}, \ell) = \frac{1}{\left[1 + \exp\left\{\frac{2\pi}{\hbar\omega_\ell}(V_{B\ell} - E_{cm})\right\}\right]} \quad (13)$$

where $V_{B\ell}$, $\hbar\omega_\ell$ are ℓ -dependent interaction barrier height, barrier width respectively. The frequency ω_ℓ which is related to the interaction barrier is calculated by applying parabolic approximation at the top of interaction barrier by using the equation given below,

$$V_T(R) = V_{B\ell} - \frac{1}{2}\mu\omega_\ell^2(R - R_{B\ell})^2 \quad (14)$$

where $R_{B\ell}$ is ℓ -dependent barrier position and μ is the reduced mass of fusing nuclei.

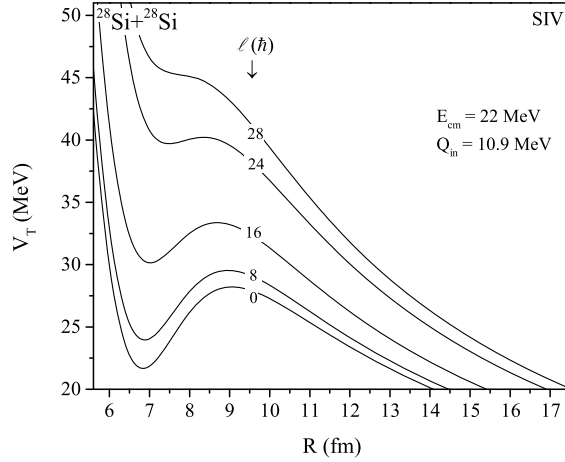


Fig. 1. The nuclear potential as function of separation distance (R) of overlapping nuclei at a center of mass-energy (E_{cm}) = 22 MeV, for different angular momentum, for SIV force.

3. Results and discussion

In this section first we have calculated the total nuclear potential as function of separation distance (R) of overlapping nuclei. Then the properties of calculated total interaction potential (barrier height, its position, and the barrier width) are used in calculation of the fusion cross sections. The fusion cross sections are calculated for different values of angular momentum for the energies near, above and below the interaction barrier. Firstly, as for angular momentum $\ell > 26\hbar$ the pocket in potential vanishes the calculation is obtained by adding the fusion cross section up to $\ell_{max} = 26\hbar$. Then fusion cross-sections are summed upto that value of angular momentum which it fits the experimental data [1,6] using HW approximation. Then the calculated fusion cross-section is compared with experimental data by taking $\ell_{max} = 38\hbar$ as predicted in ref. [2] for this system.

For calculating fusion cross-section, we have calculated all the barrier properties, obtained by using parabolic approximation at the top of barrier, which in turn is a function of angular momentum at a given center of mass energy and then so obtained properties are used to obtain the fusion cross section using HW approximation at that energy. Then the calculations are extended over the entire available energy range. However in another way, only barrier height is taken as a function of angular momentum where as other two properties are assumed to be independent of angular momentum based on the approximation used in refs [2,16].

Fig. 1 shows the calculated nuclear potential for a positive Q-value system $^{28}\text{Si}+^{28}\text{Si}$ at $E_{cm} = 22$ MeV, for Skyrme force SIV. The nuclear potential is calculated at different angular momentum. From the Fig. 1 the following changes in the total interaction potential are observed with the increase in angular momentum, (i) the separation among the successive barriers is increasing and hence the barrier height increases (ii) slight shift in the position of the barrier toward the left side of interaction barrier ($V_B(\ell = 0)$) i.e. it decreases with increase in ℓ (iii) and as a consequences of change in latter two properties causes the change in barrier curvature/width, which is calculated using parabolic approximation. It is also observed that the potential pocket disappear at $\ell = 28\hbar$. Therefore we have obtained the fusion cross section upto maximum angular momentum, $\ell_{max} = 26\hbar$.

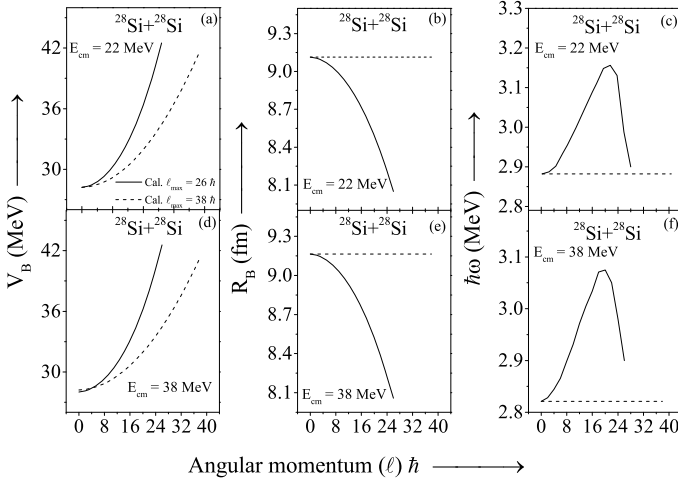


Fig. 2. The barrier properties (barrier height, barrier position, barrier curvature) of total nuclear potential as function of angular momentum at two different center of mass-energy i.e. at $E_{cm} = 22$ MeV, upper panel and $E_{cm} = 38$ MeV, lower panel, for SIV force.

The changes in the barrier properties can be seen clearly to depend upon the angular momentum at a given center of mass energy in Fig. 2. In the figure [2], properties of the barrier (barrier height (V_B), position (R_B), and the barrier curvature/width ($\hbar\omega$)) are plotted versus angular momentum at two different center of mass energies which are far below i.e. at $E_{cm} = 22$ MeV (upper panel) and far above the Coulomb barrier ($\equiv V_{B0}$) i.e. at $E_{cm} = 38$ MeV (lower panel). The solid line shows the calculated barrier properties by taking maximum angular momentum $\ell_{max} = 28\hbar$ while the dashed line shows the calculations with $\ell_{max} = 38\hbar$, which is based on assumption that is used in refs. [2,16], where the angular momentum dependent barriers were parameterized by taking barrier width and barrier position independent of angular momentum. From the figures [2(a)&(d)], it is clear that the dashed line start deviating from the solid line with increase in angular momentum which indicates that at given angular momentum the barrier height predicted from assumption based from refs. [2,16] is comparatively less as predicted from the calculation for $\ell = 28\hbar$ shown by solid line. From the figures [2(b)&(e)] and [2(c)&(f)] it is observed that the position of the barrier and its curvature depends upon angular momentum (shown with solid line) where as these are treated constant in refs. [2,16], shown with dash line.

Further it is also observed that with increase in the angular momentum the position of the barrier shifts toward left end of Coulomb barrier and this shift is shown by lowering in the position of the barrier, see figure [2(b)&(e)] and the barrier curvature increases, see [2(c)&(f)] upto certain value of angular momentum and then start decreasing. The barrier properties, based on the total nuclear potential, are also function of temperatures i.e. see eqn. (11) because in the calculations of the total interaction potential the nuclear potential is obtained within the semiclassical extended Thomas-Fermi approach of SEDF using sudden approximation where the nuclear density used is two parameter Thomas-Fermi density. The parameters are taken from ref [13], while their temperature dependence is taken from ref. [14]. On comparing these barrier properties at two different center of mass energies for a given angular momentum it is observed that with increase in the center of mass energy the height of the barrier decreases whereas the position of the barrier increases. The decrease in barrier width is also observed with increase in E_{cm} .

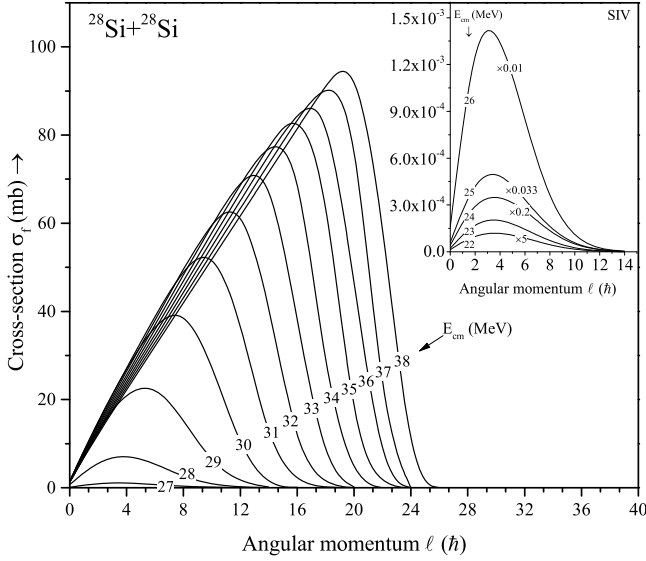


Fig. 3. The calculated fusion cross-section as a function of angular momentum using HW approximation at different center of mass energy, for SIV force.

Next we have calculated the fusion cross-section as a function of angular momentum using HW approximation. Since, in HW approximation at a given energy the penetration probability depends upon the angular momentum and hence the corresponding fusion cross-section can be calculated. Figure [3] shows the calculated fusion cross-section versus angular momentum at different E_{cm} . In the figure [3], the inset shows the plot of fusion cross-section at low energies which are far below the Coulomb barrier. Since at these low energies the calculated fusion cross-section is very low, in order to show the comparative variation the fusion cross-section at different energies the calculated fusion cross-section are shown in inset. In the inset figure, fusion cross-section calculated at $E_{cm} = 22$ MeV is multiplied with a factor of 5, similarly at other energies the cross-sections are multiplied with some other factor (can be seen in inset figure). From figure [3] it is quite clear that at given E_{cm} the fusion cross-section increase upto certain value of angular momentum (which we called σ_{max}) and then start decreasing with the increase in angular momentum. It is found that rate of the increase in the fusion cross-section which further depends upon angular momentum is almost linear upto σ_{max} and then start decreasing rapidly at higher E_{cm} . However the same is not observe at low E_{cm} , where the rate of increase as well decrease in fusion cross-section is almost same. It is observed that angular momentum corresponding to σ_{max} is increases with increase in E_{cm} . The variation of σ_{max} with the center of mass energy and the corresponding variation in the angular momentum can be plotted simultaneously. This variation is shown in the figure [4].

Then the calculations are obtained for the summed up fusion cross section for maximum angular momentum $\ell = 26\hbar$ (dashed line) and are compared with the experimental data [1,6] which is shown in Fig. 5. It is observed that at low energies it is in good agreement while at E_{cm} above and below the barrier it is not able to reproduce the data.

Further, fusion cross-section is summed upto $\ell = 38\hbar$ (dotted line), based on the assumption used in [2,16], and compared with experimental data. It almost showed the same variation as shown for $\ell = 26\hbar$ but showing slight deviation at deep sub barrier energies. Therefore calculated

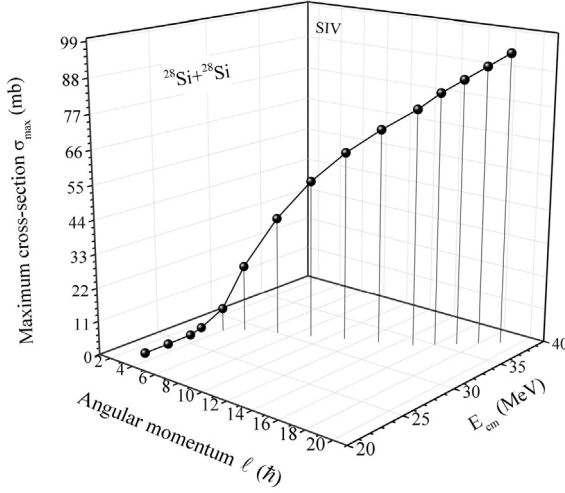


Fig. 4. The variation in maximum cross-section (σ_{max}) (solid spheres) along z-axis, as function of center of mass-energy along y-axis and the corresponding angular momentum along x-axis is shown, for SIV force.

fusion cross section is added upto that value of ℓ , called ℓ_{max} , which almost reproduces the observed data at a given E_{cm} , shown by the solid line in Fig. 2. The required angular momentum at different E_{cm} is shown in the inset of Fig. 2.

The comparative study showed that at $E_{cm} \approx 25$ MeV, the fusion cross section is relatively small and become very small above $\ell_{max} = 12\hbar$, thus further addition of the angular momentum dependent i.e. upto $26\hbar$ have no effect on the summed up fusion cross section. However, for energies above 25 MeV i.e. above and near the barrier the cross section has relatively significant contribution from both below and above $\ell = 12\hbar$, hence we need different ℓ_{max} at different E_{cm} , lower than $26\hbar$.

4. Conclusion

We have calculated the fusion cross sections based on the properties of total interaction potential by adding centrifugal potential to the nuclear proximity potential and we found that so obtained potential able to reproduce the experimental data within experimental limits of error over the entire energy range by adding suitable value of angular momentum without any fitting. It is found that properties of total interaction potential i.e. barrier width and barrier position, which plays important role in the calculation fusion cross-section varies sufficiently with change in angular momentum which were assumed to be constant in refs. [2,16]. The maximum in cross-section is observed at particular value of angular momentum which is not equal to ℓ_{max} , at given center of mass-energy and it increases with increase in E_{cm} . The cross-section which is calculated at angular momentum below angular momentum ($\ell = 28\hbar$) reproduce the experimental data very well at energies far below the barrier, however it is overestimating the data close and above Coulomb barrier. The same behavior is observed for $\ell = 38\hbar$ indicating that addition of large angular momentum have very small effect on fusion cross-section at low energy range while it significantly affect the same at higher energies. However at energies far above interaction barrier for $\ell = 0$, large value of ℓ_{max} is required to reproduce the observed data but close to the

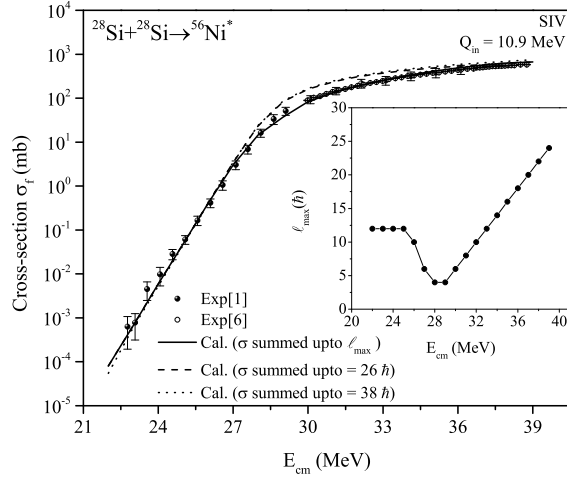


Fig. 5. The comparison of the calculated fusion cross-section as a function of E_{cm} with the experimental data [1,6] at different ℓ_{max} (solid line), at ($\ell_{max} = 26\hbar$) (dashed line) and with the assumption used in Refs. [2,16] at $\ell_{max} = 38\hbar$. The variation of maximum angular momentum which fitted the experimental data with in the experimental limits of error the center of mass energy is shown in inset figure.

barrier energy (V_{BO}) comparatively small value of ℓ_{max} is required. In future studies, we try to incorporate the role of deformations.

CRediT authorship contribution statement

The whole concept, and graphs, are prepared by author Atul Choudhary. Author VKN writes a manuscript. BSK and AKJ read the whole manuscript.

Declaration of competing interest

The authors declare that they have no known competing financial interests or personal relationships that could have appeared to influence the work reported in this paper.

Data availability

Data will be made available on request.

References

- [1] G. Montagnoli, A.M. Stefanini, et al., Phys. Rev. C 90 (2014) 44608.
- [2] H. Esbensen, Phys. Rev. C 85 (2012) 064611.
- [3] Y. Nagashima, et al., Phys. Rev. C 33 (1986) 176.
- [4] S. Gary, C. Volant, Phys. Rev. C 25 (1982) 1877.
- [5] M.F. Vineyard, et al., Phys. Rev. C 41 (1990) 1005.
- [6] G. Montagnoli, A.M. Stefanini, et al., Phys. Lett. B 300 (2015).
- [7] D.S. Verma, A. Choudhary, IJMPE-D-16-00104R1, 2016.
- [8] B. Grammaticos, A. Voros, Ann. Phys. 129 (1980) 153.
- [9] M. Brack, C. Guet, H.B. Hakansson, Phys. Rep. 123 (1985) 275.

- [10] J. Bartel, K. Bencheikh, Eur. Phys. J. A 14 (2002) 179.
- [11] P. Chattopadhyay, R.K. Gupta, Phys. Rev. C 30 (1984) 1191.
- [12] J. Blocki, J. Randrup, W.J. Swiatecki, C.F. Tsang, Ann. Phys. NY 105 (1977) 427.
- [13] R.K. Gupta, Dalip Singh, R. Kumar, W. Greiner, J. Phys. G, Nucl. Part. Phys. 36 (2009) 075104.
- [14] S. Shlomo, J.B. Natowitz, Phys. Rev. C 44 (1991) 2878.
- [15] D.L. Hill, J.A. Wheeler, Phys. Rev. 89 (1953) 1102.
- [16] C.Y. Wong, Phys. Rev. Lett. 31 (1973) 766.
- [17] D. Vautherin, D.M. Brink, Phys. Rev. C 5 (1972) 626.
- [18] J. Friedrich, P.G. Reinhardt, Phys. Rev. C 33 (1986) 335.